Electronic, structural, and magnetic properties of the half-metallic ferromagnetic quaternary Heusler compounds CoFeMnZ (Z = Al, Ga, Si, Ge)

Vajiheh Alijani, Siham Ouardi, Gerhard H. Fecher, Jürgen Winterlik, S. Shahab Naghavi, Xeniya Kozina, Gregory Stryganyuk, and Claudia Felser

Institut für Anorganische und Analytische Chemie, Johannes Gutenberg-Universität, D-55099 Mainz, Germany

Eiji Ikenaga

Japan Synchrotron Radiation Research Institute, SPring-8, Hyogo 679-5198, Japan

Yoshiyuki Yamashita, Shigenori Ueda, and Keisuke Kobayashi

NIMS Beamline Station at SPring-8, National Institute for Materials Science, 1-1-1 Kouto, Sayo-cho, Sayo-gun, Hyogo 679-5148, Japan

(Received 10 June 2011; revised manuscript received 18 October 2011; published 19 December 2011)

The quaternary intermetallic Heusler compounds CoFeMnZ (Z = Al, Ga, Si, or Ge) with 1 : 1 : 1 : 1 stoichiometry were predicted to exhibit half-metallic ferromagnetism by *ab initio* electronic structure calculations. The compounds were synthesized using an arc-melting technique and the crystal structures were analyzed using x-ray powder diffraction. The electronic properties were investigated using hard x-ray photoelectron spectroscopy. The low-temperature magnetic moments, as determined from magnetization measurements, follow the Slater-Pauling rule, confirming the proposed high spin polarizations. All compounds have high Curie temperatures, allowing for applications at room temperature and above.

DOI: 10.1103/PhysRevB.84.224416 PACS number(s): 81.05.Zx, 85.75.−d, 75.20.En, 73.22.Pr

I. INTRODUCTION

Ternary intermetallic Heusler compounds X_2YZ, where X and Y are transition or rare-earth metals and Z is a main-group element, are exceptional for their large variety of properties, ranging from half-metallic ferromagnetism over thermoelectrics to superconductivity.[1–4] Many of these properties are highly useful for technical applications, including half-metallic ferromagnetism, magnetic shape memory, and giant magnetocaloric effects, as well as implementation in spin torque transfer–random access memories (STT-MRAMs).[5–8] Half-metallic ferromagnets exhibit 100% spin polarization at the Fermi energy (ϵ_F) (Ref. 9) and have therefore been proposed as ideal candidates for spin-injection devices. In the past two decades, several different classes of materials besides Heusler compounds have been predicted to exhibit half metallicity.[10–13] Several quaternary—or, better, pseudoternary—Heusler compounds have been designed in order to tailor the middle of the gap exactly to the Fermi energy, as in $Co_2Mn_{1-x}Fe_xSi$.[14] Quaternary Heusler compounds with a 1 : 1 : 1 : 1 stoichiometry, however, have as yet been little explored, to the best of our knowledge. For symmetry reasons (T_d), they are substantially different from the $L2_1$ pseudoternary Heusler compounds with O_h symmetry and $2 : [(1-x) : x] : 1$ or $2 : 1 : [(1-y) : y]$ stoichiometry.

The $L2_1$ Heusler structure (space group $Fm\bar{3}m$) consists of four interpenetrating fcc lattices. If each of the sublattices is occupied by different atoms, a quaternary Heusler structure with changed symmetry is obtained, the so-called LiMgPdSn or Y-type structure (space group $F\bar{4}3m$).[15,16] This class of materials offers an enormous variety of possibilities for rational material design since Heusler compounds are known to exhibit tunable magnetic and electronic properties depending on their valence-electron count. Some quaternary Heusler compounds have been recently proposed to exhibit half-metallic ferromagnetism.[17] A comprehensive study of four quaternary half-metallic ferromagnetic Heusler compounds will be presented in the following. The compounds were identified by *ab initio* electronic structure calculations. The preferred route for predicting a different quaternary half metal has been to combine two ternary half metals that are already known to crystallize in the Heusler structure, such as Co_2FeSi or Co_2MnSi.[18] Following this route, the quaternary compound CoFeMnSi was identified to be a half-metallic ferromagnet.[19] The present paper reports on the theoretical identification and the experimental characterization of the quaternary Heusler half-metallic ferromagnets CoFeMnZ (Z = Al, Ga, Si, Ge). In applications, the quaternary CoFeMnZ compounds will have advantages over the pseudoternary $Co_2Fe_{1-x}Mn_xZ$ alloys. In the latter case, i.e., the alloy type, random distribution of Fe and Mn leads to additional disorder scattering resistivity and thus to an increase in the total resistivity. The result is that electronic devices based on *real* quaternary Heusler compounds are expected to have lower-power dissipations.

The experimental results presented in the following include a structural analysis by powder x-ray diffraction (XRD), a characterization of the magnetic properties by a superconducting quantum interference device (SQUID), and an investigation of the electronic structure by hard x-ray photoelectron spectroscopy (HAXPES).

II. EXPERIMENT

CoFeMnZ (Z = Al, Ga, Si, Ge) bulk samples were prepared by repeated arc melting of stoichiometric amounts of high-purity constituents in an argon atmosphere. To avoid oxygen contamination, a Ti sponge was used as an oxygen absorber before melting the compounds. The samples were melted three times from both sides to ensure sufficient homogeneity. The resulting polycrystalline ingots were annealed in evacuated quartz tubes for 2 weeks at 1073 K, and then quenched in a bath

containing an ice and water mixture. Flat disks were cut from the ingots and polished for spectroscopic investigations of the bulk samples. The crystal structure was investigated by means of XRD using Mo $K\alpha$ radiation (Bruker D8 Advance) and the magnetic properties by means of SQUID magnetometry (Quantum Design, MPMS-XL-5) using small spherical sample pieces of ∼20–30 mg.

For the HAXPES measurements, polished disks of the samples were fractured *in situ* in an ultrahigh-vacuum chamber before the respective measurements to avoid surface contamination as a result of air exposure. The experiments were carried out at the beamlines BL15XU (Ref. 20) and BL47XU of SPring-8. At BL15XU, the photon energy was fixed at 5.9534 keV using an Si (111) double-crystal monochromator (DCM) and the 333 reflection of a Si channel cut postmonochromator. At BL47XU, the photon energy was fixed at 7.9392 keV using a Si(111) DCM and the 444 reflection of the channel cut postmonochromator. At both beamlines, the photoelectrons were analyzed and detected by means of hemispherical analyzers (VG Scienta, R4000). The overall energy resolution (monochromator plus analyzer) was set to 240 meV, as verified by spectra of the Au valence band at ϵ_F. Additionally, spectra were recorded with a resolution of 150 meV. The angle between the electron spectrometer and photon propagation was fixed at 90°. The photons were p polarized, i.e., the electric field vector is in the plane of incidence and always points in the direction of the electron detector. A nearly normal emission ($\theta \approx 2°$–$5°$) angle was used for electron detection. (Note that the angle is not that well defined for fractured bulk samples because of surface roughness.) The measurements were performed at sample temperatures of 300 K. The core-level spectra were analyzed using the program UNIFIT 2011.[21]

III. RESULTS AND DISCUSSION

A. Structural properties

The classical intermetallic Heusler compounds consist of two transition or rare-earth elements and one main-group element in the stoichiometric composition X_2YZ, and they crystallize in the cubic $L2_1$ structure (space group 225: $Fm\bar{3}m$). When one of the two X atoms is substituted by a different transition metal X', a quaternary compound with the composition $XX'YZ$ and $F\bar{4}3m$ symmetry (space group 216) is generated. The prototype of this Y-type structure of quaternary Heusler compounds is LiMgPdSn.[15,22] Three possible nonequivalent superstructures based on the different positions of the four atoms exist for this structural type[23] (see Table I). As shown in Fig. 1, the LiMgPdSn-type structure exhibits a primitive fcc cell with a basis containing four atoms on the Wyckoff positions 4a to 4d, which form a larger cubic cell. The three nonequivalent primitive or cubic cells are explained in Table I for the example of CoFeMnSi, as depicted in Fig. 1. It is known from the corresponding regular Heusler compounds Co_2MnZ or the archetype Cu_2MnAl (Ref. 24) that the Mn atoms and the main-group elements are typically located on the octahedrally coordinated a and b Wyckoff positions, identical to the situation in type I in Table I. This configuration determines highly localized magnetic moments at the Mn atoms, which dictate the magnetic order in Heusler compounds.[25]

TABLE I. Different site occupations for the Y-type structure. M denotes a main-group element. Note that exchange of atoms between the 4a and 4b or 4c and 4d positions and between the groups (4a,4b) ↔ (4c,4d) does not change the structure because of the symmetry implied by the $F\bar{4}3m$ space group. In $L2_1$, the positions (4c,4d) become equivalent and combine to 8c.

	4a (0,0,0)	4c (1/4,1/4,1/4)	4b (1/2,1/2,1/2)	4d (3/4,3/4,3/4)
Y type I	M	Fe	Mn	Co
Y type II	M	Mn	Fe	Co
Y type III	Fe	M	Mn	Co

The XRD patterns of the compounds, measured at room temperature, are shown in Fig. 2. Rietveld refinements of the data were performed using the TOPAS ACADEMIC software package.[26] Details of the refinements are shown in Table II. In the patterns of CoFeMnGa and CoFeMnGe, the (111) and (200) fcc superstructure reflections are very small or completely absent. This is the result of the nearly equal scattering amplitudes of all the constituent elements (3d and 4p); this impedes a detailed order-disorder analysis by Mo $K\alpha$ XRD. It is impossible to distinguish among types I, II, and III (see Table I) for all compounds because only 3d elements are involved. For the Rietveld refinements, type I was assumed, based on the experiences from regular X_2YZ Heusler compounds and the results of the *ab initio* electronic structure calculations (see Sec. III B). However, an analysis of order was possible for the Al and Si atoms. In the pattern of CoFeMnAl, the (200) reflection is clearly visible, but (111) is not visible at all. This indicates disorder among the Mn and Al atoms when type I is assumed. Including this type of structural disorder in the refinement provided an improved weighted-profile R factor R_{wp} of 10.90%, as compared to 12.62% for an assumed ordered Y-type structure. It has been known for several years that Al-containing Heusler compounds are very susceptible to

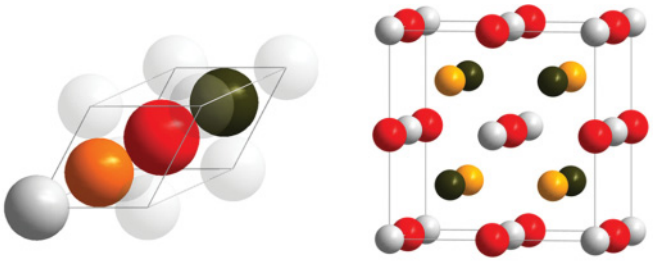

FIG. 1. (Color online) Crystal structure of the quaternary Y-type Heusler compound CoFeMnSi and related primitive cell. There are three nonequivalent supercells of CoFeMnSi in the Y-type structure, depending on the occupation of the four different lattice sites 4a (0,0,0), 4b (1/2,1/2,1/2), 4c (1/4,1/4,1/4), and 4d (3/4,3/4,3/4). As deduced from ternary Heusler compounds, Co and Fe should occupy the lattice sites 4c and 4d, and Mn and Si should occupy 4b and 4a. Si atoms are gray, Co atoms are orange (medium gray), Fe atoms are brown (dark gray), and Mn atoms are red (atoms with larger radius). The ratios of atomic radii correspond to the factual values of the atoms.

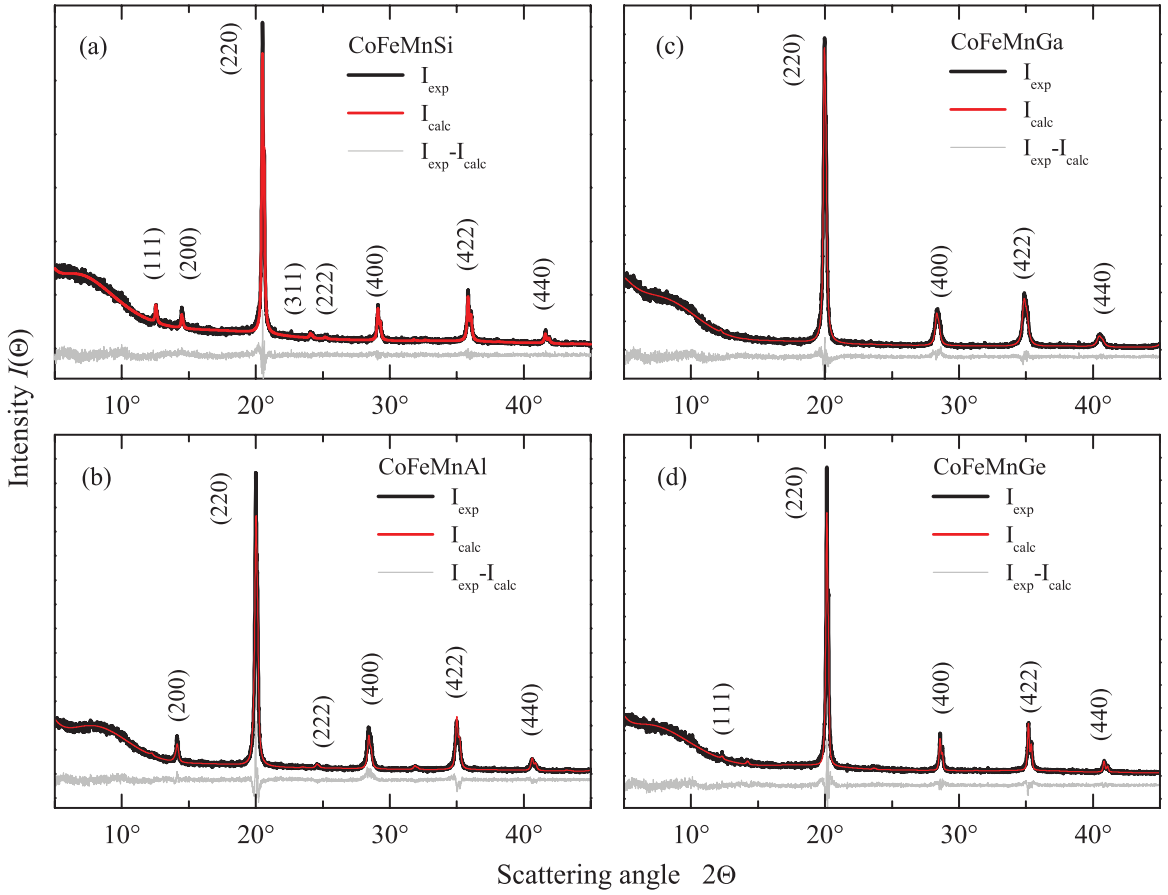

FIG. 2. (Color online) Powder XRD and Rietveld refinements of CoFeMnZ [Z = Al (a), Si (b), Ga (c), and Ge (d)]. The measurements were carried out at room temperature using Mo $K\alpha$ radiation.

this type of disorder.[27] Similarly, but to a smaller extent of disorder (≈15% for Mn and Si), the Rietveld refinement of CoFeMnSi was improved (R_{wp} = 8.38%, Y type: 8.50%).

B. Electronic structure calculations

Ab initio electronic structure calculations were performed using WIEN2k (Refs. 28–30) and the generalized gradient approximation (GGA).[31] The number of plane waves was restricted by $R_{MT}k_{max} = 9$. All self-consistent calculations were performed with 256 k points in the irreducible wedge of the Brillouin zone, based on a mesh of 20^3 k points. The density of states was calculated on a mesh of 25^3 k points.

TABLE II. Lattice parameters and weighted-profile R factors R_{wp} of CoFeMnZ compounds. The lattice parameters a_{exp} and a_{calc} are given in Å. a_{calc} is taken from a structural optimization (see Sec. III B). The R factors R_{wp} of CoFeMnAl and CoFeMnSi were determined using disordered structural models, as described in the text.

Z	a_{exp} (Å)	a_{calc} (Å)	R_{wp} (%)
Al	5.786	5.692	10.90
Si	5.655	5.610	8.38
Ga	5.811	5.708	10.52
Ge	5.763	5.710	10.70

The convergence criteria were set to 10^{-5} Ry for energy and simultaneously to $10^{-3}e^-$ for charges. It was checked that the energies were converged with respect to the number of k points and the number of plane waves. Further details are given in Refs. 17 and 32. The lattice parameters were optimized as a starting point for the calculation of the band structures, densities of states, and magnetic moments. The magnetic state was checked by use of different settings of the initial magnetization: ferromagnetic (all initial spins parallel) or ferrimagnetic (initial spins partially antiparallel). The results of the structural optimization are summarized in Table III. In the case of the type III atomic arrangements, two different magnetic ground states were found. The additional results (marked by *) exhibit higher energies compared to the other magnetic and site configurations. For the type I and II atomic arrangements, only one magnetic ground state was found, independent of the initial settings of the magnetization.

All structural optimizations showed that the type I structures with Co(4d)Fe(4c)Mn(4b)Z(4a) exhibit the lowest energy, as reported in detail for CoFeMnSi (Ref. 19) (the small differences in the results are caused by the larger number of plane waves used in the present paper). The total energy of the type I structure is on average ≈270 meV lower than that of the type II structure. The optimized lattice parameters are compared with the experimental values in Table II. GGA usually tends to slightly larger lattice parameters. It

TABLE III. Results of the structural optimization. Total energies E_{tot} are in Ry, lattice parameters a_{opt} are in Å, and magnetic moments m are in μ_B. The structure types are explained in Table I. For the "*" types different settings of the initial magnetization were used.

	E_{tot}	a_{opt}	m_{tot}	m_{Co}	m_{Fe}	m_{Mn}
CoFeMnAl						
Type I	−8135.602 20	5.692	3.00	0.81	−0.13	2.44
Type II	−8135.577 82	5.775	5.03	1.20	2.22	1.76
Type III	−8135.569 80	5.793	6.41	1.80	2.11	2.66
Type III*	−8135.540 59	5.772	0.68	1.21	2.03	−2.46
CoFeMnSi						
Type I	−8230.066 30	5.611	4.00	0.89	0.52	2.70
Type II	−8230.044 94	5.613	3.98	0.95	2.52	0.58
Type III	−8230.013 37	5.649	5.33	1.81	1.66	1.98
Type III*	−8230.004 33	5.588	0.45	0.47	1.58	−1.51
CoFeMnGa						
Type I	−11538.167 10	5.717	3.05	0.77	−0.25	2.60
Type II	−11538.156 19	5.792	5.98	1.26	2.45	2.42
Type III	−11538.147 72	5.832	6.84	1.79	2.28	2.87
Type III*	−11538.122 54	5.810	0.35	1.22	2.11	−2.88
CoFeMnGe						
Type I	−11848.126 62	5.713	4.01	0.86	0.51	2.71
Type II	−11848.101 52	5.726	4.25	0.99	2.54	0.81
Type III	−11848.076 47	5.780	6.03	1.75	1.94	2.45
Type III*	−11848.066 34	5.756	0.18	−0.48	−1.81	2.39

is obvious that all calculated values are ≈1% below the experimental values. This may be attributed to a temperature effect (measurement at 300 K), to disorder, and/or other structural defects. In the following, type I structures with optimized lattice parameters were used for the calculations of the electronic structures and magnetic properties of the compounds.

The stability of the cubic structure was checked by calculation of the elastic constants c_{ij}. The elastic constants were calculated by applying isotropic strain as well as volume-conserving tetragonal and rhombohedral strains to the optimized cubic primitive cell. There are only three independent components for cubic symmetry: $c_{11} = c_{22} = c_{33}$, $c_{12} = c_{13} = c_{23}$, and $c_{44} = c_{55} = c_{66}$. The bulk modulus of cubic systems is derived from $B = (c_{11} + 2c_{12})/3$. The elastic stability criteria of the cubic structure are found from the elastic constants.[33] For stability of the cubic structure, the bulk modulus, the c_{44} shear modulus, and the tetragonal shear modulus must be positive, resulting in the following conditions: $c_{11} + 2c_{12} > 0$, $c_{44} > 0$, and $c_{11} - c_{12} > 0$.

The elastic anisotropy $A_e = 2c_{44}/(c_{11} - c_{12})$ compares the shear moduli and allows a decision about the structural stability. The Young's modulus becomes isotropic for $A_e = 1$. Materials with large A_e ratios show a tendency to deviate from the cubic structure. The results of the calculated elastic properties are summarized in Table IV. The results are for the Birch-Murnaghan equation of state (EOS). They are within ≈±0.4 GPa compared to EOS2 (Ref. 34) or Murnaghan, and no differences in the optimized lattice parameters are observed within 10^{-4} Å for different EOSs. All fits to determine the optimized lattice parameters were performed with nine volume changes between −8% and +8% approximately around the relaxed volume. For elastic properties, seven deformations within ±4% about the equilibrium structure were used.

TABLE IV. Elastic constants of CoFeMnZ compounds (Z = Al, Si, Ga, Ge). All values of the elastic constants c_{ij} and the bulk moduli B are given in GPa; A_e is dimensionless.

Z	c_{11}	c_{12}	c_{44}	B	A_e
Al	212	178	167	189	9.7
Si	317	189	167	231	2.6
Ga	198	183	158	188	20.5
Ge	263	178	156	206	3.5

CoFeMnGa exhibits the lowest bulk modulus, and the highest values are observed for CoFeMnSi and CoFeMnGe. With respect to both A_e and the elastic stability criteria, the compounds are stable in the cubic Y-type crystal structure. The observed structural instability of CoFeMnAl, with a tendency to disorder,[23] may be related to the comparatively high elastic anisotropy. The Cauchy pressure ($p_C = c_{12} - c_{44}$) is positive for all four compounds.

Figures 3–6 show the calculated electronic structures of the CoFeMnZ (Z = Al, Si, Ga, Ge) compounds. The compounds exhibit electronic structures typical of fully spin-polarized half-metallic ferromagnetic Heusler compounds with a band gap in the minority channel.

All compounds exhibit a typical Heusler-compound hybridization gap between the low-lying s bands and the remaining high-lying part of the valence bands, which mainly contains p and d states. The sizes of the sp gap of the compounds differ but do not depend much on the spin character of the bands because of the small exchange splitting of the s states. The hybridization gaps between W and L are indirect, and their sizes are 40 meV, 1 eV, 1.7 eV, and 2.6 eV for Z = Al, Ga, Si, and Ge, respectively. The widths of the low-lying s bands are 3.5, 2.5, 3, and 2.5 eV for Al, Si, Ga, and Ge, respectively. This is related to the different lattice parameters and thus to the differences in the overlaps of the wave functions. The small sp gap in CoFeMnAl points to weak

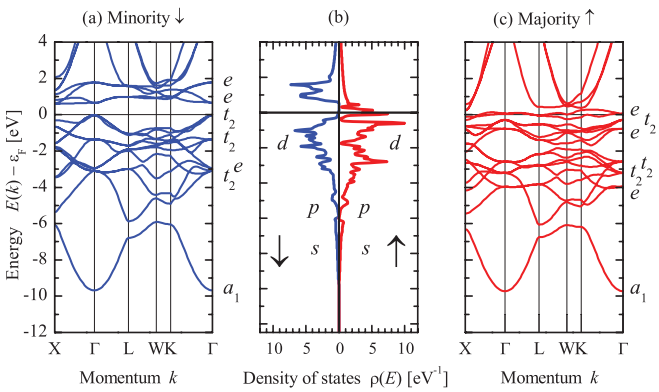

FIG. 3. (Color online) Band structures and densities of states of CoFeMnAl: (a) minority bands, (b) densities of states, and (c) majority bands. Majority- and minority-spin densities are denoted by ↑ and ↓, respectively. The irreducible representations of the bands are given for the Γ point.

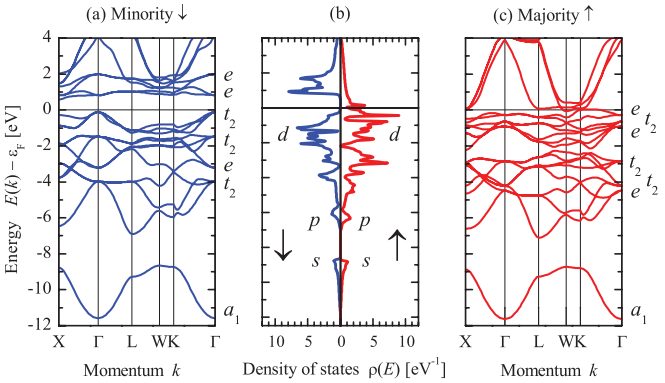

FIG. 4. (Color online) Band structures and densities of states of CoFeMnSi: (a) minority bands, (b) densities of states, and (c) majority bands. Majority- and minority-spin densities are denoted by ↑ and ↓, respectively. The irreducible representations of the bands are given for the Γ point.

hybridization and indicates structural instability; this may be the reason for antisite disorder.

The most important feature of the electronic structure is the band gap in the minority channel, turning the compounds to half-metallic ferromagnets. This band gap in the minority states arises from a particular band filling by 12 valence electrons. This is caused by successive filling of the minority bands a_1 by one s electron, t_2 by three p electrons, e and t_2 by a total of five d electrons, followed by subsequent complete filling of an additional t_2 band by three d electrons (see the assignment of the irreducible representations of the bands at Γ in Figs. 3 and 4 for the example of the compounds based on Al and Si, respectively). It should be noted that the representations for the T_d group used here for the quaternary compounds with a 1 : 1 : 1 : 1 composition are considerably different from quaternary (pseudoternary) or ternary Heusler compounds with O_h symmetry and a 2 : 1 : 1 composition described in Ref. 35. At 24 valence electrons, a quasi-closed-shell character is reached, accounting for both spin channels with 12 minority and 12 majority electrons. Additional valence electrons (here three for Al, Ga, or four for Si, Ge) fill majority bands only, and the exchange interaction concurrently splits the minority and majority bands. According to the Slater-Pauling rule,[36,37] ϵ_F is pinned directly above the occupied minority states. In

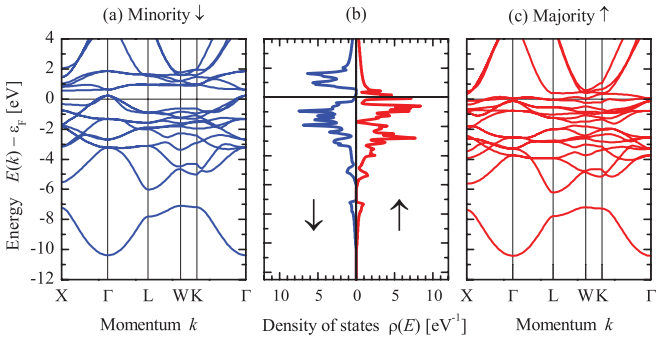

FIG. 5. (Color online) Band structures and densities of states of CoFeMnGa: (a) minority bands, (b) densities of states, and (c)) majority bands. Majority- and minority-spin densities are denoted by ↑ and ↓, respectively.

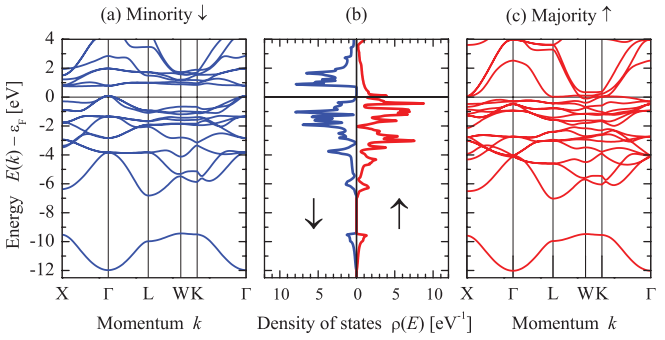

FIG. 6. (Color online) Band structures and densities of states of CoFeMnGe: (a) minority bands, (b) densities of states, and (c)) majority bands. Majority- and minority-spin densities are denoted by ↑ and ↓, respectively.

the minority channel of CoFeMnGa, 0.02 electrons are found above ϵ_F at the optimized lattice parameter, calculated for $T = 0$ K. A slight change in the lattice parameter will push this band at the Γ point away from ϵ_F. It is interesting to note that these states will be depleted at elevated temperatures as a result of the Fermi-Dirac distribution; this increases the spin polarization with temperature.

C. Magnetic properties

The magnetic properties of the polycrystalline samples were investigated using a SQUID magnetometer. The field-dependent magnetization at 5 K is shown in Fig. 7. The corresponding magnetic moments at saturation are given in Table V. Although the magnetic moment of CoFeMnSi is in reasonable accordance with the Slater-Pauling rule,[38–40] the other compounds exhibit higher magnetic moments than expected. These results indicate the existence of disorder and/or magnetic impurities. As is known from the structural characterizations, disorder was identified in CoFeMnAl and CoFeMnSi, and cannot be excluded for CoFeMnGa and CoFeMnGe. Magnetic impurities were not identified in either

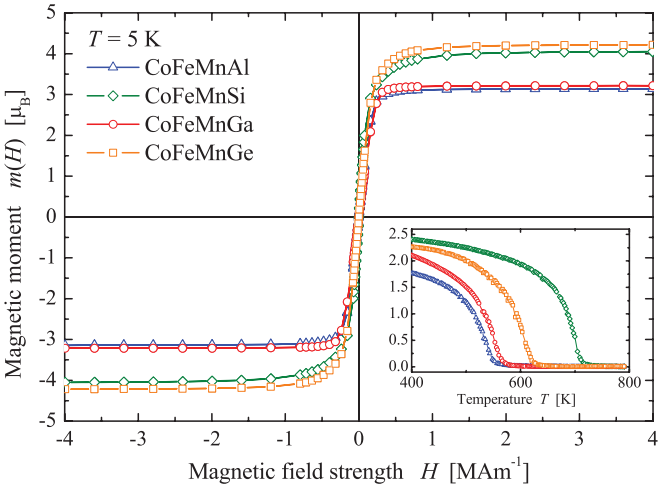

FIG. 7. (Color online) Magnetic properties of CoFeMnZ (Z = Al, Si, Ga, and Ge). The field-dependent measurements were performed at T = 5 K. The inset shows temperature-dependent magnetic moments in the high-temperature range of the Curie temperature.

TABLE V. Magnetic moments and T_C values of CoFeMnZ compounds. The moments are given in μ_B, and the temperatures in K.

Z	m_{exp}(5 K)	m_{exp}(300 K)	m_{calc}	T_C
Al	3.1	2.7	3.0	553
Si	4.1	3.7	4.0	623
Ga	3.2	2.8	3.0	567
Ge	4.2	3.8	4.0	711

of the diffraction patterns but may be below the detection limit of XRD, i.e., an impurity content of ≈5%. The Curie temperatures T_C of the compounds were determined by temperature-dependent magnetization measurements, as shown in the inset of Fig. 7 and in Table V. Evidently, all compounds exhibit high T_C, facilitating technological applications.

The calculated values m_{calc} of the total magnetic moments are all integers, as is typical for half-metallic ferromagnets with a band gap in the minority states at ϵ_F. According to the Slater-Pauling rule, the magnetic moments adopt values of $3\mu_B$ for $Z =$ Al and Ga, and $4\mu_B$ for $Z =$ Si and Ge. From the calculations of the site-specific moments, it is evident that the magnetic properties are mainly determined by the Mn atoms, which contribute the highest magnetic moments, of $\sim 2.5\mu_B$. The magnetic moment at the Co sites is also stable against variations of the Z element and the number of valence electrons. It exhibits a value of $\sim 0.8\,\mu_B$. Most interestingly, the moment at the Fe site shows the strongest variation and even exhibits a change of sign when comparing compounds with 27 and 28 valence electrons. In CoFeMnAl and CoFeMnGa, it is oriented antiparallel to the Mn and Co atoms. This may be interpreted as a ferrimagnetic order. The nearest neighbors of Mn are Co and Fe atoms. It can therefore be supposed that the magnetic moments at the Fe atoms are induced by the neighboring Mn spins. In other words, the stability of the Co and Mn moments, together with the Slater-Pauling rule, dictates whether the moment at the Fe sites is aligned antiparallel or parallel to Mn. This obvious dependence of the Fe moments also explains the soft-magnetic behavior of the compounds, even for seemingly ferrimagnetic types of order. A detailed investigation of the local magnetic moments of these compounds has recently been carried out using x-ray magnetic circular dichroism and supports the findings shown here.[41]

The measured magnetic moments at 5 K are increased by $0.1\mu_B$ for the Al and Si compounds, and by $0.2\mu_B$ for the Ga and Ge compounds, as compared to the calculated values. Evidently, the magnetic order is conserved at room temperature, and the temperature dependences of the magnetic moments for all compounds are very similar.

D. Hard x-ray photoelectron spectroscopy

The compounds with $Z =$ Si and Ge were investigated using photoelectron spectroscopy. The measurements were carried out at different excitation energies in order to investigate the influence of varying cross sections.

1. Core-level spectroscopy

Figure 8 shows the HAXPES spectra of CoFeMnSi and CoFeMnGe in the energy range of the semicore level (note the low intensity of the valence band at energies from −12 eV to 0 compared to the intense Ge 3*s* or Si 2*s* lines). The spin-orbit splitting of the 3*p* states is resolved clearly for Ge, but not for the transition metals (Co, Fe, Mn), despite the small differences in nuclear charges.

Besides the spin-orbit splitting of the *p* states, the spectra shown in Fig. 8 exhibit several satellites, which have different origins. The appearance of metallic satellites (for example, plasmons) or multiplet splittings resulting from exchange interactions is typical. The spin-orbit (Δ_{SO}) and exchange (Δ_{EXC}) splittings were determined for selected core and semicore levels. Selected results for Δ_{SO} are summarized in Table VI. The most interesting finding is that the Mn 3*s* states of the compounds exhibit well-distinguished exchange splittings of $\Delta^{\mathrm{Si}}_{\mathrm{EXC}} = 4.3$ eV and $\Delta^{\mathrm{Ge}}_{\mathrm{EXC}} = 4.6$ eV [see Fig. 8(b)]; these splittings are quite independent of the main-group element or the total magnetic moment. The intensity ratio between the main 3*s* line and the exchange-split satellite appears to be independent of the photon energy; it

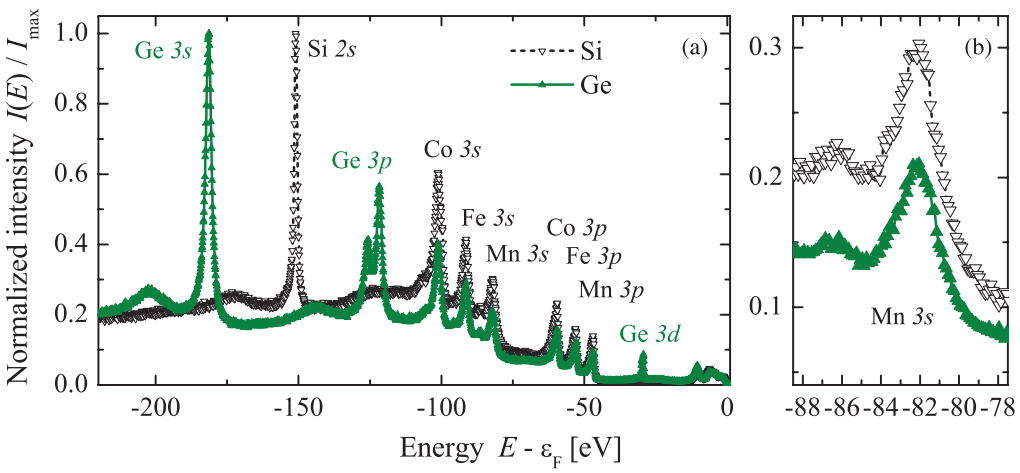

FIG. 8. (Color online) Spectra of the shallow core states of CoFeMnZ ($Z =$ Si, Ge). The excitation energy was $h\nu = 7.9380$ keV. The spectra are normalized to the maxima for easier comparison; (b) shows an enlarged view of the Mn 3*s* states.

TABLE VI. Experimentally determined spin-orbit splitting Δ_{SO} and intensity ratios in the core-level spectra of CoFeMnSi and CoFeMnGe. $R(2p_{3/2}) = I_{Co}/I_{Fe}/I_{Mn}$ is the intensity ratio of the $2p_{3/2}$ core states. B is the branching ratio of the $2p$ states. All core-level energies are given in eV. The exact excitation energies $h\nu = 5.9534$ and 7.9380 keV are denoted by 6 and 8, respectively.

		Co $2p$		Mn $2p$		Fe $2p$		
Z	$h\nu$	Δ_{SO}	B	Δ_{SO}	B	Δ_{SO}	B	$R(2p_{3/2})$
Si	6	14.90	2.30	11.96	3.07	13.00	3.15	1 : 1.09 : 1.07
	8		1.83		2.91		2.76	
Ge	6	15.00	2.42	11.80	3.49	13.00	3.29	1 : 1.08 : 1.06
	8		2.03		3.25		3.01	

amounts to 1.37 ± 0.01. The Coulomb interaction of the Mn $3s$ core hole and the Mn $3d$ valence electrons leads to a splitting of the photoionized state into sublevels[35,42] caused by the existence of more than one possible final ionic state during ejection of electrons, even from a closed s shell. A difference in the splitting would point to differences in the localization of the Mn $3d$ valence electrons in CoFeMnSi and CoFeMnGe. The observed similarity of the compounds shows that the Mn atoms behave identically and independently of the main-group element, even though the compounds differ in their total magnetic moments.

Figure 9 displays the results of the core-level photoemissions from the transition-metal $2p$ states of CoFeMnSi and CoFeMnGe excited by hard x rays of energy ~6 keV. The typical spin-orbit splitting of the states into $2p_{1/2}$ and $2p_{3/2}$ sublevels is clearly detected.

The details of the spin-orbit splitting of the transition-metal $2p$ core levels are summarized in Table VI, together with selected intensity ratios. The intensity ratio $R(2p_{3/2}) = I_{Co}/I_{Fe}/I_{Mn}$ of the $2p_{3/2}$ core states is independent of the compound and points to the correct stoichiometry of the samples. The statistical branching ratio $B = I(2p_{3/2})/I(2p_{1/2})$ is expected to be 4 : 2 from the $(2j + 1)$ multiplicity of the states. In nearly all cases, the observed branching ratios are larger than the statistical value of 2. At the higher photon energy of ~8 keV, they are lower than those measured at the

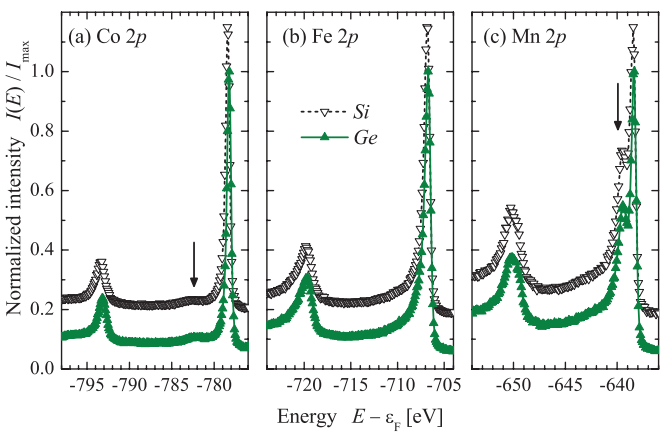

FIG. 9. (Color online) Co, Fe, and Mn $2p$ core levels of CoFeMnZ (Z = Si, Ge). The most important satellites (see text) are marked by arrows. The photon energy was $h\nu = 5.9534$ keV.

excitation energy of ~6 keV. This is because of the energy dependence of the differential cross sections σ_{nlj} and angular asymmetry parameters β_{nlj}.[43] For the present experimental setup and linearly p-polarized photons, the energy dependence of the branching ratio for the $2p$ states is given by

$$B(E) = \frac{\sigma_{2p_{3/2}}(E)[1 + \beta_{2p_{3/2}}(E)]}{\sigma_{2p_{1/2}}(E)[1 + \beta_{2p_{1/2}}(E)]}. \quad (1)$$

This ratio only accounts for the spin-orbit-split components and does not include multiplet effects. The changes in the branching ratios with excitation energy, however, reflect the energy dependence of both the differential cross section and the angular asymmetry parameter.

The observed spin-orbit splitting itself is independent of the excitation energy, as expected. The calculated spin-orbit splittings are 14.8, 12.5, and 10.4 eV for Co, Fe, and Mn, respectively. These values are within 10 meV, independent of the main-group element in the CoFeMnZ compounds. The observed and calculated values for Co and Fe are in good agreement within the resolution of the experiment. A considerable deviation is found for the Mn $2p$ states (≈1.5 eV). The reason is the observed multiplet splitting (see below), which was not accounted for in the calculations. The interaction between the core hole and the valence electrons in the photoexcited state causes an additional increase in the splitting on top of the ground-state spin-orbit interaction.

A pronounced, further splitting of the Fe $2p$ states is not observed. The absence of multiplet effects in the Fe $2p$ states points to the *weak* role of the Fe atoms in the magnetic properties of the compounds, as discussed above. In both compounds, the Co $2p_{3/2}$ state exhibits a broad satellite at ~4 eV below the maximum [marked by an arrow in Fig. 9(a)]. This satellite is also seen in the Co $2p_{1/2}$ state. The Co $2p$ satellite may be the result of an intra-atomic shakeup transition from states directly below ϵ_F into the onset of the unoccupied s bands at ~4–5 eV above ϵ_F. An influence of the interaction between the core hole with the partially filled d bands cannot, however, be excluded. A similar transition is also observed in x-ray absorption spectroscopy and is assigned to effects of the fcc structure.[41,44]

The Mn $2p_{3/2}$ state exhibits a typical multiplet structure with a pronounced splitting of ~1 eV [see the arrow in Fig. 9(c)]. This splitting is not seen in the Mn $2p_{1/2}$ state but leads only to a considerable broadening of the line. Additional weaker satellites show up as broadenings at ~4 and 7 eV below the Mn $2p_{3/2}$ and $2p_{1/2}$ states, respectively. The multiplet splitting of the Mn $2p$ states arises from the interaction of the core hole with the partially filled d bands, which are strongly localized.[45,46] Similar to the splitting of the Mn $3s$ state, the Coulomb interactions of the Mn $2p$ core holes and the Mn $3d$ valence electrons lead to splitting caused by the existence of several possible final ionic states.[35,42] The splittings and intensity ratios observed in the spectra of the Mn states of CoFeMnGe or CoFeMnSi are very close to those of Co_2MnGe. In Ref. 35, the multiplet splittings of the Mn $3s$ and $2p$ states were analyzed in detail and it was shown, by comparing experimental data with calculations, that the Mn state cannot be identified as being definitely ionic Mn^{3+} or Mn^{2+}, but is in between. This means that one has either a mixture of d^4

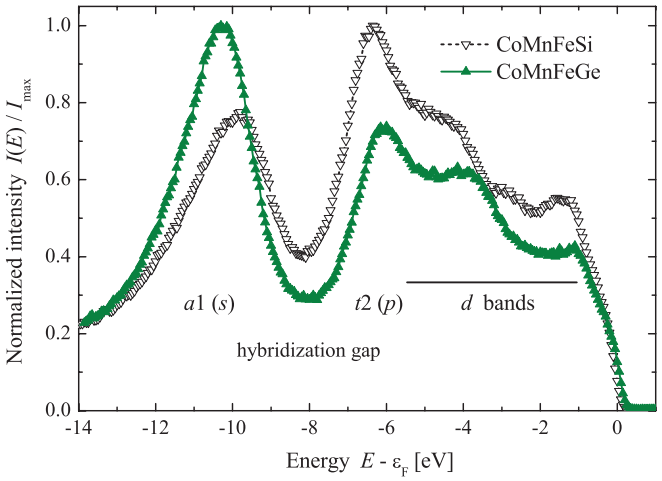

FIG. 10. (Color online) HAXPES valence-band spectra of CoFeMnSi and CoFeMnGe. The excitation energy was set at $h\nu = 7.9380$ keV. For easier comparison, the spectra are normalized to their maxima.

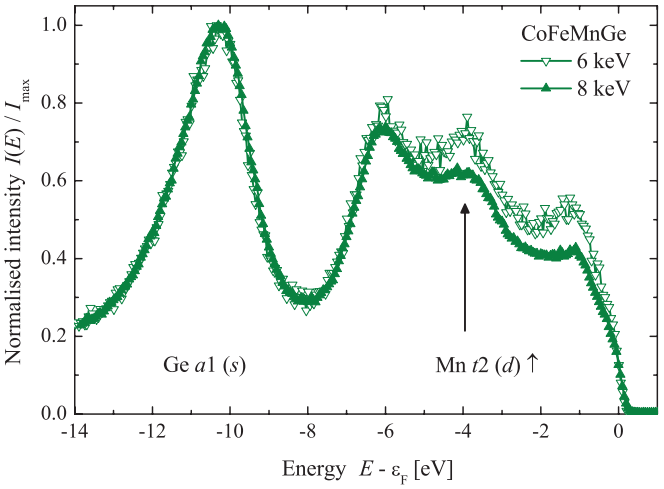

FIG. 11. (Color online) Valence-band spectra of CoFeMnGe at different excitation energies.

and d^5 or, more realistically for a metallic solid, a formal $d^{4.x}$ configuration with respect to the incomplete localization of the d electrons at the Mn site.

2. *Valence-band spectroscopy*

Figure 10 compares the valence-band spectra of CoFeMnSi and CoFeMnGe excited by hard x rays of photon energy of ∼8 keV. Both compounds exhibit the hybridization gap expected from the electronic structure calculations at ∼8 eV below ϵ_F. The low-lying s states with a_1 character at Γ exhibit maxima at −9.9 and −10.5 eV for CoFeMnSi and CoFeMnGe, respectively. The energies of the maxima correspond to the middle of the low-lying a_1 bands rather than to the maxima in the calculated densities of states at −8.9 and −9.6 eV (see Figs. 4 and 6). As a result of the different cross sections for the Si 3s and Ge 4s states at the same photon or kinetic energy, the intensity is considerably lower in CoFeMnSi than in CoFeMnGe. At the same time, the maxima at ∼−6 eV are lower in CoFeMnGe than in CoFeMnSi.

The energy range of the d bands in CoFeMnSi contains three major maxima at ∼−1.55, −2.95, and −4.4 eV. A comparison with the calculated densities of states reveals that they arise from localized d states, either at Fe or Mn, which are responsible for the localized magnetic moments in Heusler compounds. The Co d states appear to be rather delocalized. Only two major maxima related to d states are resolved for CoFeMnGe at −1.3 and −4.1 eV. The maximum at −4.1 eV arises mainly from t_2 majority states localized at the Mn atoms. The states at ∼−1.55 eV or −1.3 eV are in both compounds localized to a greater extent at Fe than at Mn. Overall, the valence-band spectra of both compounds show good agreement with the calculated densities of states using GGA. This shows that the localizations of the Fe and Mn d states are rather insensitive to the type of order or disorder. It should also be noted that no pronounced effects of electron-electron correlations are observed. Figure 11 compares the valence-band spectra of CoFeMnGe excited by hard x rays of different energies. With increasing photon energy, the cross section of the s states decreases more slowly compared to the d states. The intensity in the energy range of the d bands is, at the lower photon energy, increased compared to the range of the s bands. Both the intensity arising from the Mn t_2 majority states at ∼−4.1 eV and that arising from the d states at −1.3 eV become more pronounced at the lower excitation energy.

IV. SUMMARY

In summary, the quaternary intermetallic Heusler compounds CoFeMnZ (Z = Al, Ga, Si, or Ge) were identified as potential half-metallic ferromagnets with high T_C by *ab initio* electronic structure calculations. The compounds were then synthesized, and the electronic and structural properties were analyzed at 300 K, and the magnetic properties were analyzed at 5 K. All the compounds exhibit cubic Heusler structures. A certain amount of disorder was found in the XRD patterns of CoFeMnAl and CoFeMnSi, and cannot be excluded for CoFeMnGa and CoFeMnGe, as a result of the similar scattering amplitudes of the corresponding elements. A detailed study of order-disorder is required to clarify the complex crystallographic situation with four equivalent fcc sublattices. Anomalous XRD and extended x-ray absorption fine structure (EXAFS) studies will help to clarify this. It was, however, shown for related and recently reported quaternary half-metallic ferromagnetic Heusler compounds that disorder does not influence the electronic structures to an extent that destroys the half metallicity[17] of the compounds.

Bulk sensitive hard x-ray photoelectron spectroscopy revealed the correct compositions of CoFeMnSi and CoFeMnGe. The multiplet splitting of the Mn 3s and 2p states suggests incomplete localization, i.e., a metallic character of the d electrons in the compounds. The absence of multiplet effects in the Fe 2p states points to a weak role for Fe in the magnetic properties of the compounds, in agreement with the electronic structure calculations. Observed changes in the spectra (for valence bands) on the one hand and similarities (for core levels) on the other when changing the excitation energy are exclusively the result of differences in the cross sections. This rules out surface influences for kinetic

energies of 5 keV and above. The energy dependences of cross sections and angular asymmetry parameters are revealed in the energy dependence of the $2p$ branching ratios of all three transition-metal elements.

The magnetic moments of the compounds are in fair agreement with the Slater-Pauling rule, indicating the half metallicity and high spin polarization required for spintronics applications. The results are also in accordance with the electronic structure calculations and the results of x-ray magnetic circular dichroism.[41] The Mn atoms carry the highest local magnetic moments and, together with the Co atoms and the Slater-Pauling rule, dictate the orientation of the Fe moments. The Curie temperatures of all compounds are higher than 550 K, allowing use at room temperature and above. The many possible combinations in designing quaternary 1 : 1 : 1 : 1 Heusler compounds give enormous potential for many applications such as in spintronics or thermoelectrics and other areas of research, and clearly deserve further exploration in the future.

ACKNOWLEDGMENTS

This work was financially supported by the *Deutsche Forschungs Gemeinschaft* DfG (projects TP 1.2-A and TP 1.3-A of Research Unit *ASPIMATT* FOR 1464) and DfG-JST (FE633/6-1). The HAXPES measurements at SPring-8 were performed at BL47XU with the approval of the Japan Synchrotron Radiation Research Institute (JASRI) (Long-term Proposal 2008B0017) and at BL15XU with the approval of NIMS (Nanonet Support Proposal 2008B4903). S.N. and X.K. acknowledge support by the Graduate School of Excellence MAINZ-MATCOR. The authors are grateful to HiSOR, Hiroshima University, and JAEA/SPring-8 for the development of HAXPES at BL15XU of SPring-8.

[1] S. Wurmehl, G. H. Fecher, H. C. Kandpal, V. Ksenofontov, C. Felser, H. J. Lin, and J. Morais, Phys. Rev. B **72**, 184434 (2005).
[2] J. Barth, L. M. Schoop, A. Gloskovskii, A. Shkabko, A. Weidenkaff, C. Felser, H. J. Lin, and J. Morais, Z. Anorg. Allg. Chem. **636**, 132 (2010).
[3] J. Winterlik, G. H. Fecher, C. Felser, M. Jourdan, K. Grube, F. Hardy, H. von Löhneysen, K. L. Holman, and R. J. Cava, Phys. Rev. B **78**, 184506 (2008).
[4] J. Winterlik, G. H. Fecher, A. Thomas, and C. Felser, Phys. Rev. B **79**, 064508 (2009).
[5] J. Winterlik, B. Balke, G. H. Fecher, C. Felser, M. C. M. Alves, F. Bernardi, and J. Morais, Phys. Rev. B **77**, 054406 (2008).
[6] C. Felser, G. H. Fecher, and B. Balke, Angew. Chem., Int. Ed. Engl. **46**, 668 (2007).
[7] S. Wurmehl, H. C. Kandpal, G. H. Fecher, and C. Felser, J. Phys. Condens. Matter **18**, 6171 (2006).
[8] K. Ullakko, J. K. Huang, and C. Kantner, Appl. Phys. Lett. **69**, 1966 (1996).
[9] R. A. de Groot, F. M. Mueller, P. G. van Engen, and K. H. J. Buschow, Phys. Rev. Lett. **50**, 2024 (1983).
[10] J. Kübler, A. R. William, and C. B. Sommers, Phys. Rev. B **28**, 1745 (1983).
[11] K. Schwarz, J. Phys. F **16**, L211 (1986).
[12] M. Nakao, Phys. Rev. B **74**, 172404 (2006).
[13] K.-I. Kobayashi, T. Kimura, H. Sawada, K. Terakura, and Y. Tokura, Nature (London) **395**, 677 (1998).
[14] B. Balke, G. H. Fecher, H. C. Kandpal, C. Felser, K. Kobayashi, E. Ikenaga, J.-J. Kim, and S. Ueda, Phys. Rev. B **74**, 104405 (2006).
[15] U. Eberz, W. Seelentag, and H. U. Schuster, Z. Naturforsch. B **35**, 1341 (1980).
[16] H. Pauly, A. Weiss, and H. Witte, Z. Metallkunde **59**, 47 (1968).
[17] V. Alijani, J. Winterlik, G. H. Fecher, S. S. Naghavi, and C. Felser, Phys. Rev. B **83**, 184428 (2011).
[18] H. C. Kandpal, G. H. Fecher, C. Felser, and G. Schönhense, Phys. Rev. B **73**, 094422 (2006).
[19] X. Dai, G. Liu, G. H. Fecher, C. Felser, Y. Li, and H. Liu, J. Appl. Phys. **105**, 07E901 (2009).
[20] S. Ueda, Y. Katsuya, M. Tanaka, H. Yoshikawa, Y. Yamashita, S. Ishimaru, Y. Matsushita, and K. Kobayashi, in *Proceedings of the 10th International Conference on Synchrotron Radiation Instrumentation*, edited by R. Garrett, I. Gentle, K. Nugent, and S. Wilkins, AIP Conf. Proc. No. 1234 (AIP, Melville, NY, 2010), p. 403.
[21] R. Hesse, T. Chasse, and R. Szargan, Fresen J. Anal. Chem. **365**, 48 (1999).
[22] J. Drews, U. Eberz, and H.-U. Schuster, J. Less-Common Met. **116**, 271 (1986).
[23] G. E. Bacon and J. S. Plant, J. Phys. F **1**, 524 (1971).
[24] F. Heusler, Verh. Dtsch. Phys. Ges. **5**, 219 (1903).
[25] J. Winterlik, S. Chadov, V. Alijani, T. Gasi, K. Filsinger, B. Balke, G. H. Fecher, C. A. Jenkins, J. Kübler, G. D. Liu, L. Gao, S. S. P. Parkin, and C. Felser, (Unpublished).
[26] A. Coelho, TOPAS ACADEMIC, version 4.1, 2007.
[27] B. Balke, S. Wurmehl, G. H. Fecher, C. Felser, and J. Kübler, Sci. Technol. Adv. Mater. **9**, 014102 (2008).
[28] P. Blaha, K. Schwarz, P. Sorantin, and S. B. Tricky, Comput. Phys. Commun. **59**, 399 (1990).
[29] P. Blaha, K. Schwarz, G. K. H. Madsen, D. Kvasnicka, and J. Luitz, *WIEN2k, An Augmented Plane Wave + Local Orbitals Program for Calculating Crystal Properties* (Karlheinz Schwarz, Techn. Universitaet Wien, Wien, Austria, 2001).
[30] K. Schwarz, P. Blaha, and G. K. H. Madsen, Comput. Phys. Commun. **147**, 71 (2002).
[31] J. P. Perdew, K. Burke, and M. Ernzerhof, Phys. Rev. Lett. **77**, 3865 (1996).
[32] H. C. Kandpal, G. H. Fecher, and C. Felser, J. Phys. D **40**, 1507 (2007).
[33] J. F. Nye, *Physical Properties of Crystals* (Clarendon, Oxford, UK, 1957).
[34] D. M. Teter, G. V. Gibbs, M. B. Boison, D. C. Allan, and M. P. Teter, Phys. Rev. B **52**, 8064 (1995).
[35] S. Ouardi, G. H. Fecher, B. Balke, A. Beleanu, X. Kozina, G. Stryganyuk, C. Felser, W. Klöß, H. Schrader, F. Bernardi, J. Morais, E. Ikenaga, Y. Yamashita, S. Ueda, and K. Kobayashi, Phys. Rev. B **84**, 155122 (2011).
[36] J. C. Slater, Phys. Rev. **49**, 931 (1936).
[37] L. Pauling, Phys. Rev. **54**, 899 (1938).

[38]G. H. Fecher, H. C. Kandpal, S. Wurmehl, C. Felser, and G. Schönhense, J. Appl. Phys. **99**, 08J106 (2006).
[39]J. Kübler, *Theory of Itinerant Electron Magnetism* (Oxford University Press, Oxford, UK, 2000).
[40]I. Galanakis, P. H. Dederichs, and N. Papanikolaou, Phys. Rev. B **66**, 174429 (2002).
[41]P. Klaer, B. Balke, V. Alijani, J. Winterlik, G. H. Fecher, C. Felser, and H. J. Elmers, Phys. Rev. B **84**, 144413 (2011).
[42]F. de Groot and A. Kotani, *Core Level Spectroscopy of Solids* (CRC, London, 2008).
[43]M. B. Trzhaskovskaya, V. I. Nefedov, and V. G. Yarzhemsky, At. Data Nucl. Data Tables **77**, 97 (2001).
[44]M. Kallmayer, H. Schneider, G. Jakob, H. J. Elmers, B. Balke, and S. Cramm, J. Phys. D **40**, 1552 (2007).
[45]C. S. Fadley, D. A. Shirley, A. J. Freeman, P. S. Bagus, and J. V. Mallow, Phys. Rev. Lett. **23**, 1397 (1969).
[46]S. Ouardi, B. Balke, A. Gloskovskii, G. H. Fecher, C. Felser, G. Schönhense, T. Ishikawa, T. Uemura, M. Yamamoto, H. Sukegawa, W. Wang, K. Inomata, Y. Yamashita, H. Yoshikawa, S. Ueda, and K. Kobayashi, J. Phys. D **42**, 084010 (2009).